



ELSEVIER

Journal of Materials Processing Technology 105 (2000) 204–213

Journal of  
**Materials  
Processing  
Technology**

www.elsevier.com/locate/jmatprotec

# Computational modelling of a precision optical lens polishing process on small radius spherical surfaces

J. Sun<sup>a</sup>, L.C. Zhang<sup>a,\*</sup>, Y.-W. Mai<sup>a</sup>, J.A. Gal<sup>b</sup>, M. Hogg<sup>c</sup>, S. Payor<sup>c</sup>

<sup>a</sup>Department of Mechanical and Mechatronic Engineering, Centre for Advanced Materials Technology (CAMT),  
The University of Sydney, Sydney, NSW 2006, Australia

<sup>b</sup>School of Mechatronic, Computer and Electrical Engineering, University of Western Sydney, Nepean Campus, Kingswood, NSW 2747, Australia

<sup>c</sup>Eycon Lens Laboratories Pty. Ltd., 296 Burns Bay Road, Sydney, NSW 2066, Australia

Accepted 20 June 2000

## Abstract

A thorough understanding of the mechanics of contact and friction mechanisms is of great practical importance to the process of precision optical lens polishing. The present work is aimed at modelling the polishing process for spherical optical lenses with small radii ( $r = (5.50-8.85) \times 10^{-3}$  cm). A finite element technique (ABAQUS/Standard) was employed to perform the analysis. The results include information about the contact status during the polishing process, the polishing load distribution on the contact surface and the variation of the spatial polishing trace. The problem of the missing polishing zone on the workpiece is also discussed. © 2000 Elsevier Science S.A. All rights reserved.

**Keywords:** Modelling; Finite element; Precision polishing; Optical lens; Spherical surface

## 1. Introduction

In precision optical lens polishing, when a polishing tool and a workpiece are brought together, direct and accurate measurement of the conditions at the contact surfaces is difficult. Consequently, the analysis can be evaluated only in terms of the polishing result and its acceptability under the particular processing conditions. The problem is compounded by the complex contact behaviour of the polishing tool and workpiece during the polishing process. This behaviour is sensitive to the constituent materials of the two contact bodies, the roughness profile of both surfaces, the polishing load, the direction of the load in relation to the actual contact area, the lubrication condition, as well as other factors. Although, both experimental and analytical approaches have been helpful for understanding the phenomena under different circumstances, each have certain limitations. For example, the experimental approach may be time consuming and expensive, while analytical solutions may be obtained only for simple cases. These problems have been discussed extensively [1–3], but for more complicated cases formidable mathematics are needed for formulating the very complex governing equations of the contact mechanics. However, by adopting a finite element analysis

(FEA) approach, some of the analytically indeterminate and unmeasurable contact properties can be simulated numerically using this powerful technique.

This work employed ABAQUS/Standard (Version 5.4) and the Lagrange multiplier method for the analysis procedure. The modelling work was focused on the contact status of the precision polishing process. The distribution of the polishing load over the contact surface, being of the order of a few newtons, and the spatial polishing trace on the workpiece surface during the polishing cycle, are determined by the FEA.

## 2. Modelling of optical lens polishing

### 2.1. Theoretical consideration

A schematic representation of the polishing process, consisting of the tool and the workpiece, is shown in Fig. 1. The workpiece is located on the top of a moving hemispherical surface. Two right-handed, Cartesian coordinate systems are defined, one fixed to the tool, A, the other fixed to the workpiece, B, and moving with it. In the instantaneous position shown in Fig. 1, both the fixed Z-axis and the moving z-axis, are directed to point outward, normal to the plane of the figure. The angular velocities,  $\omega_1$ ,  $\omega_2$  and  $\omega_3$ , represent the rotation of the polishing machine,

\* Corresponding author. Fax: +61-2-9351-3760.  
E-mail address: zhang@mech.eng.usyd.edu.au (L.C. Zhang).

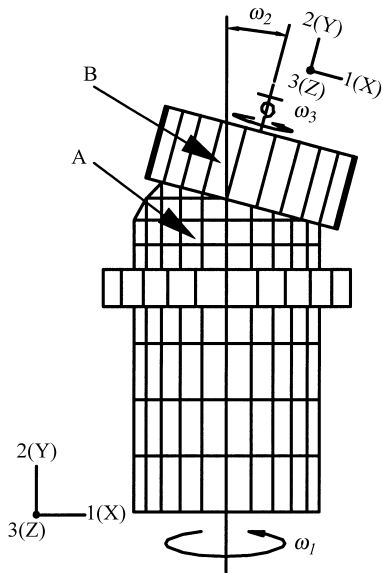


Fig. 1. Illustration of the polishing process.

the sliding motion of lens over the surface of the polishing tool, and the self-rotation velocity of the workpiece about its own axis of symmetry, the y-axis, respectively. In the computation, the model is considered to be three-dimensional.

The elastic body A, which is moving with the prescribed angular velocity  $\omega_1$ , is in contact with another elastic body B as shown in Fig. 1. To develop the governing equations for the contact conditions, it is assumed that at time  $t_0$  the surfaces of the two bodies A and B come into contact when a load is applied to the top of B. An implicit integration scheme is chosen here for the dynamic analysis [4].

In the implicit scheme using FEA, the mass matrix is formulated on the basis of consistent mass properties, and the time integration is completed by Newmark’s formula for displacement and velocity. The half-step residual is used as the time increment for the next step.

The boundary conditions given in the computation are classified into three types. They are (1) loading condition, (2) constraint condition of tool, and (3) constraint condition of workpiece. The initial conditions on the surface of the bodies A and B may be expressed as

$$\dot{u}_i^A(x, t_0) = 0, \quad \dot{u}_i^B(x, t_0) = 0$$

where  $\dot{u}_i^A$  and  $\dot{u}_i^B$  are the velocity vectors of a coincident point,  $i$ , on the bodies A and B.

The motion of the system must also satisfy all the conditions at the interface between the two bodies, including the displacement and fraction continuity on the interface surface I. Denoting by the displacement and velocity of two points, one on each body, at the interface surface as  $u_i^A, \dot{u}_i^A, u_i^B, \dot{u}_i^B$ , the contact condition can be expressed as

$$u_1^A(x, t) = u_1^B(x, t), \quad \dot{u}_1^A(x, t) = \dot{u}_1^B(x, t)$$

and the component of force per unit area, in the normal direction, between the bodies across the interface must satisfy

$$\sigma_{ij}n_j = p_i$$

The constitutive equation of the interface in this work is based on the Coulomb friction law, i.e.,

$$f_i = \mu p_i$$

where  $f_i$  is the friction force and  $\mu$  the coefficient of friction.

### 2.2. FEM simulation of the contact surface

The isotropic Coulomb friction contact model (with a shear stress cap) is employed [4]. Whether or not frictional slip occurs is determined by the value of  $\tau_{eq} = (\tau_T^2 + \tau_w^2)^{1/2}$  where  $\tau_{eq}$  is the equilibrium shear stress between the contact surfaces,  $\tau_T$  the shear stress on the tool surface and  $\tau_w$  the shear stress on the workpiece surface. When  $\tau_{eq} < \tau_{crit}$ , no relative sliding occurs and the stick-state condition is applicable; when  $\tau_{eq} = \tau_{crit}$  sliding occurs; thus frictional slip starts when  $\tau_{crit}$  is the critical shear stress between contact surfaces.

### 2.3. Element types

The selection of contact elements is based on the availability of the element models within the program library of ABAQUS/Standard. To generate a three-dimensional mesh for the contact surface, a semi-circular, three-dimensional 6-node element (IRS3-C3D6) is used for the central cycle structure and a cubic three-dimensional 8-node element (IRS13-C3D8) is used for the remaining of the structure. The two types of solid elements available are of the second-order interpolation in strain type. When the elements are used for pressure distribution analysis, the strains are calculated as the integral of the rate of deformation. The influence of material rotation with respect to the coordinate system is also taken into account. In all the situations, the stresses in each element are reported as the “true” stress [5]. Stress and strain components are referred to the global spatial directions in the fixed coordinate system.

### 2.4. Model of the contact surface

The model is generated using MSC/PATRAN (PAT 301), an FEA pre-processing package. Fig. 2 illustrates the mesh of the contact surface in a three-dimensional view. The central node number is 21, at which the normal direction is the rotation axis of the contact surface. The total number of surface nodes is 145 and total number of surface elements is 144 including 120 IRS13-C3D8 elements and 24 IRS3-C3D6 elements. The element and node details of the model are listed in Table 1.

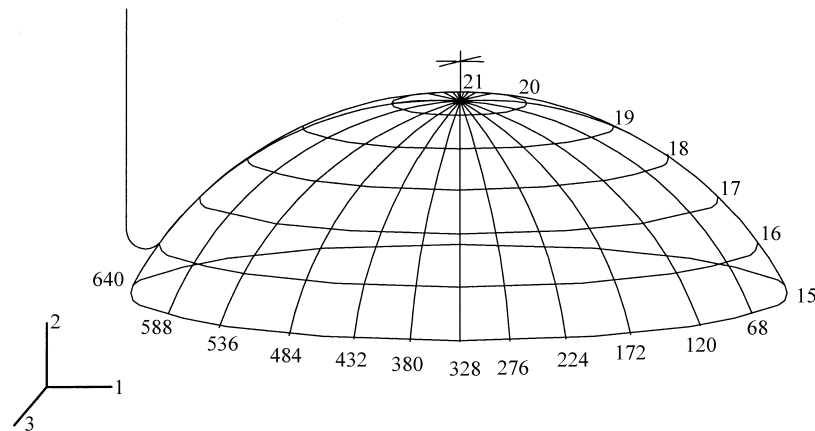


Fig. 2. Mesh of modelled contact surface.

Table 1  
Element and node details of the model

Number of elements	820
Number of elements defined by the user	385
Number of dummy elements for Lagrange multipliers	290
Number of internal elements generated for contact	145
Number of nodes	1115
Number of nodes defined by the user	583
Number of internal nodes generated by the program	532
Total number of variables in the model (degrees of freedom plus any Lagrange multiplier variables)	2916

### 3. Numerical results and discussion

The numerical results were obtained using the following polishing parameters: polishing load = 4 N,  $\omega_1 = 1200, 1350, 1500, 1650$  and  $1800$  rpm, and  $\omega_2 = 50$  rpm. The contact surface conditions were determined using different friction coefficients ( $\mu = 0.3, 0.4$  and  $0.5$ ). The radius of spherical contact surface varied within the range from  $5.5$  to  $8.9$  mm with an increment of  $0.2$  mm. The polishing parameters used are based on the experiments and analyses of actual polishing processes, and in order to maintain the practical significance of this numerical analysis, polishing parameters outside this range were not considered.

#### 3.1. Polishing load distribution on the contact surface

Figs. 3–6 display typical examples of numerical simulation results with desired settings for the polishing parameters at  $\omega_1 = 1500$  rpm,  $\omega_2 = 50$  rpm,  $\mu = 0.4$  and  $r = 7.5$  mm. Information about the polishing load distribution on the contact surface is provided by these simulation results.

The figures show changes in polishing load distribution during a single periodical span close to the start and then at 1, 2 and 3 s into running time. The cycle is repeated over the complete polishing process simulation. In the figures, the small closed loop shows a higher value of compression

pressure (the polishing load), and the greater the distance from the centre of the smallest closed loop, the lower the polishing load. It can also be seen that a higher polishing load during the polishing process has an effect at the edge of the contact surface.

It is instructive to analyse the relationship between the contact area ratio and the contact pressure from the numerical results. The ratio is defined as the loop area compared to the entire contact surface area. The loop area is obtained using the Visual-Graphic package (a computer graphical imaging program). Because the sliding angle of the workpiece is less than  $20^\circ$ , the area can be approximated by a plane, with 6% error, as being the projection of the area onto the  $X-Z$ . In the case of an apparently open loop, the edge of the contact surface forms the missing part of the boundary. Each loop represents a line of constant contact pressure corresponding to the numerical results.

Fig. 7 shows that the relationship between the contact area ratio and the contact pressure using the typical example discussed above. It can be seen that the higher the ratio, the lower the pressure. At the beginning, the situation is almost static and hence this case is not considered being not significant in the dynamic analysis. The uneven distribution on the contact surface appearing at the completion of all the polishing cycles may indicate difficulty in achieving geometrical accuracy for the workpiece and in maintaining uniform polishing quality over the whole polishing process. Some areas of the surface would be polished more harshly than others and this may explain the missing zone problem of this polishing process on a small spherical surface. Therefore, the uneven distribution of the polishing load during the polishing process probably plays a major role in giving rise to this problem. Factors due to the tooling profile may also contribute to the missing zones at the centre or the edge of the workpiece. Thus the results of the analysis can be applied for different polishing conditions, particularly for evaluating the settings of the polishing process, which affect the polishing result.

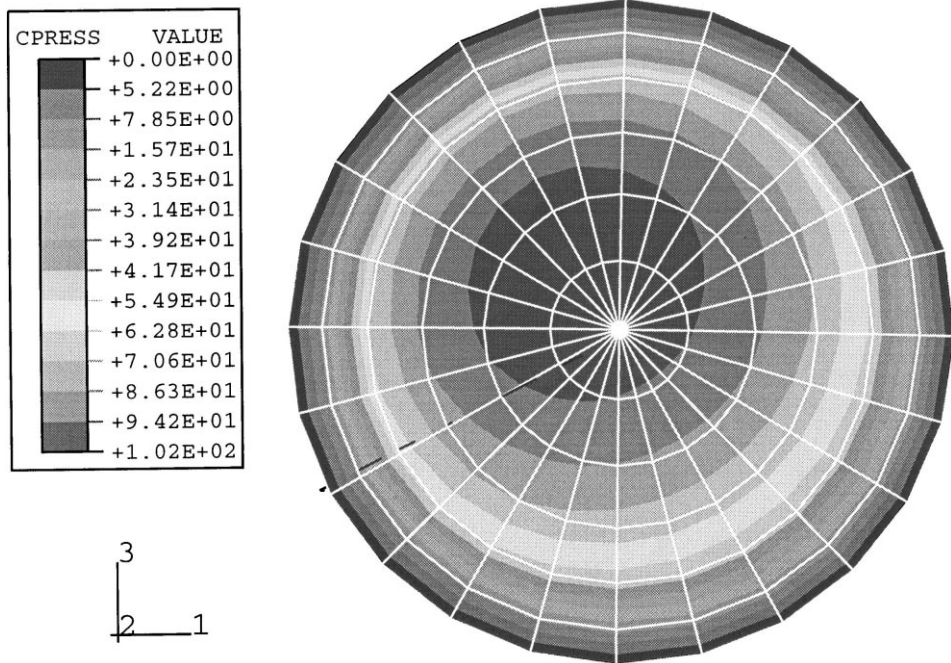


Fig. 3. Polishing pressure distribution at  $t=0.1$  s.

### 3.2. Polishing trace analysis

A single given node on the polishing tool surface generates the polishing trace on the workpiece surface. The global coordinate system is fixed on the polishing tool and the moving coordinate system is associated with the workpiece. The position of a trace point on the workpiece is

determined in terms of global coordinates. For a meaningful analysis, a comparison is now made between the trace patterns for different machine speeds based on the desired polishing parameters (refer to Figs. 15–19) and the results are evaluated.

Ideally, the motion mechanism of the polishing machine generates a figure “8” movement on the workpiece surface

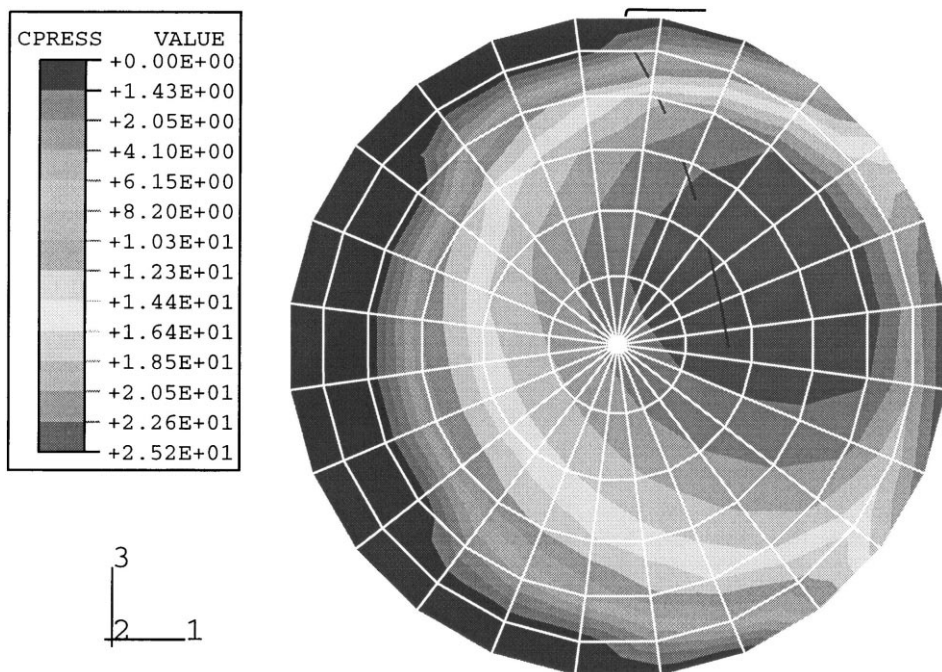


Fig. 4. Polishing pressure distribution at  $t=1.0$  s.

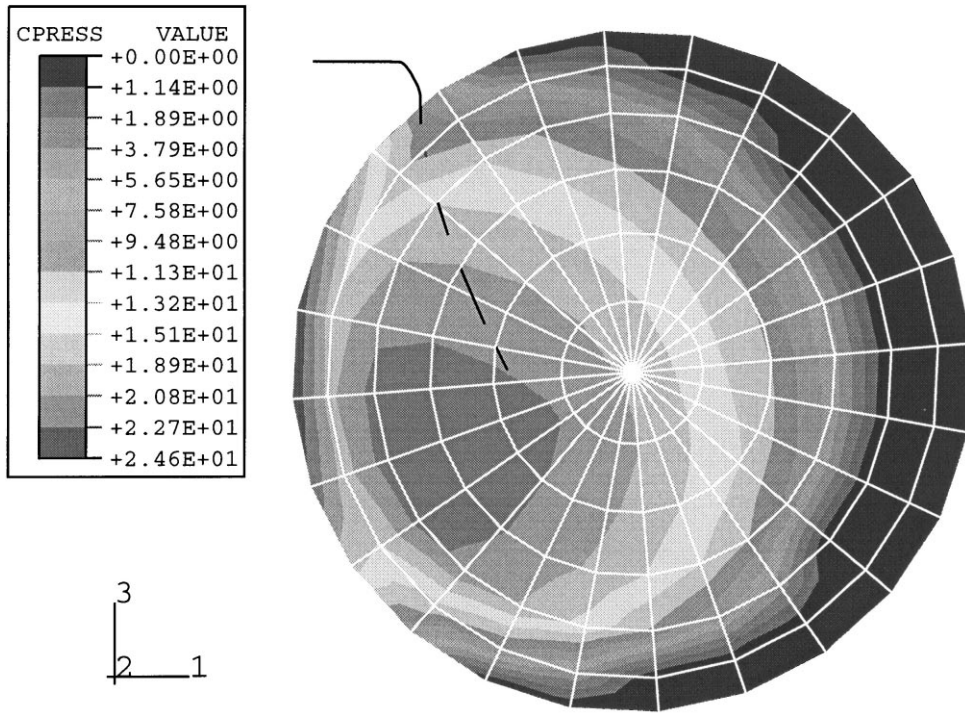


Fig. 5. Polishing pressure distribution at  $t=2.0$  s.

during the polishing. However, the actual motion is from the centre to the edge on the workpiece with light buffeting in a circular fashion around the polishing tool. The stability of the workpiece motion during the polishing process is dependent on the contact characteristics and on

the load. An evaluation of the polishing machine speed is required in considering the stability of the workpiece motion and the efficiency of the polishing process. Four points on the tool surface, *a*, *b*, *c* and *d* as indicated in Fig. 8, are employed to generate trace patterns. The polishing

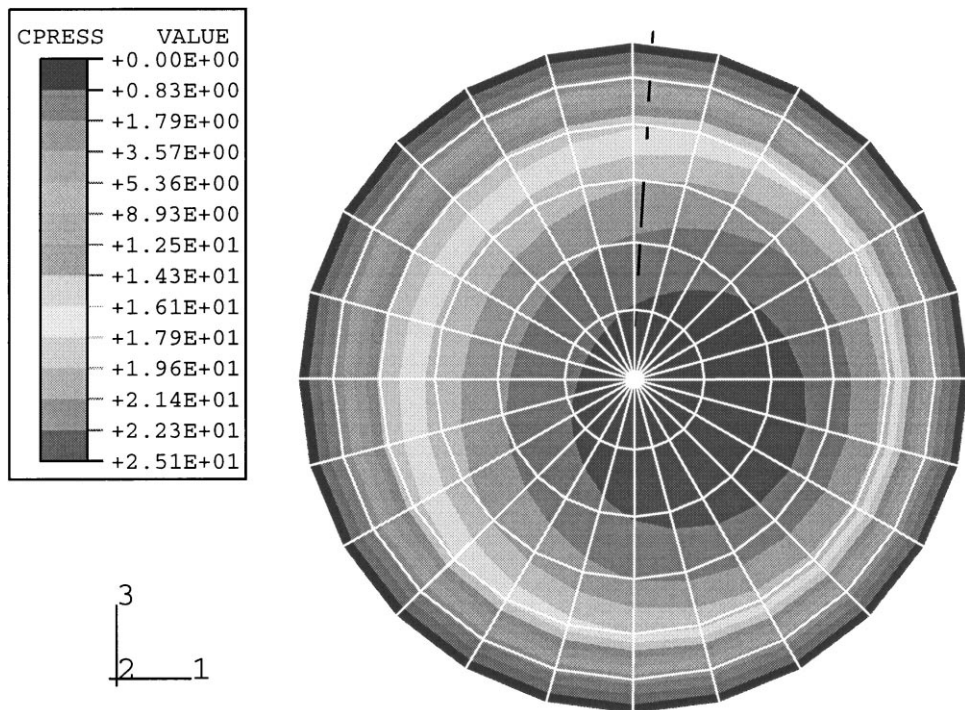


Fig. 6. Polishing pressure distribution at  $t=3.0$  s.

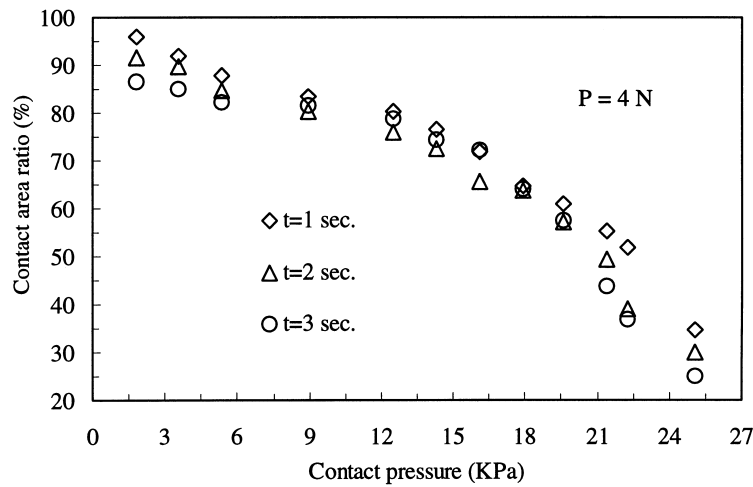


Fig. 7. Relation between contact area ratio and contact pressure.

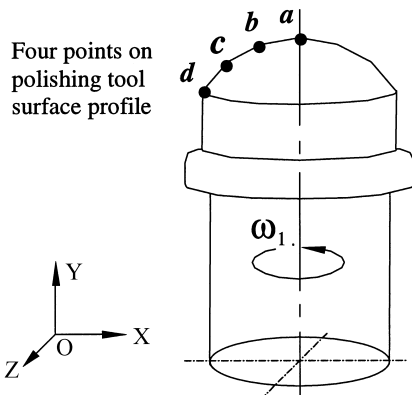


Fig. 8. Illustration of four points on polishing tool surface.

parameters used are  $\omega_1=1350$  rpm,  $\omega_2=50$  rpm,  $\mu=0.4$ ,  $P=4$  N and  $r=7.5$  mm.

Figs. 9–12 show typical polishing trace patterns on the workpiece surface produced by the four points on the polishing tool surface, respectively. The simulation running time is 60 s and the 1600 plotted points in these figures represent the positions of the trace point for that period. The polishing trace pattern is a projected view onto the X–Z plane as shown in the figures. It can be seen that the trace pattern is not really a figure “8” movement; this distortion is due to the light buffeting. The trace of the centre point *a* is more concentrated at the centre area of the workpiece, while the trace of the edge point *d* is more concentrated at the workpiece edge. The intermediate points *b* and *c* produce traces exhibiting a more even coverage over the whole area.

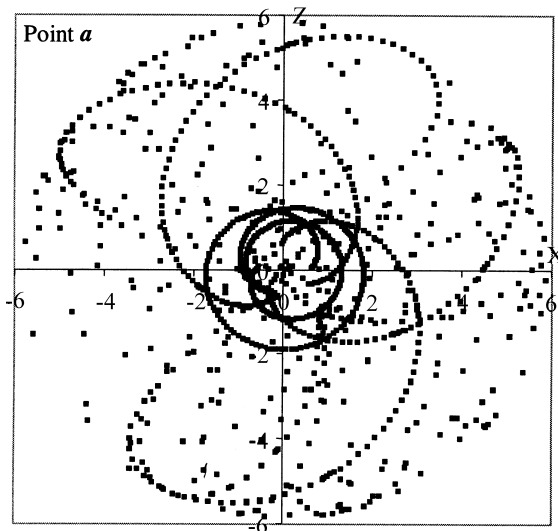


Fig. 9. The polishing trace pattern on the workpiece surface created by point *a*.

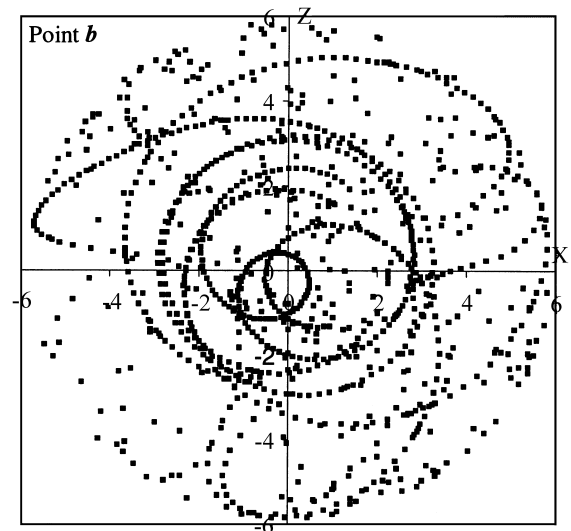


Fig. 10. The polishing trace pattern on the workpiece surface created by point *b*.

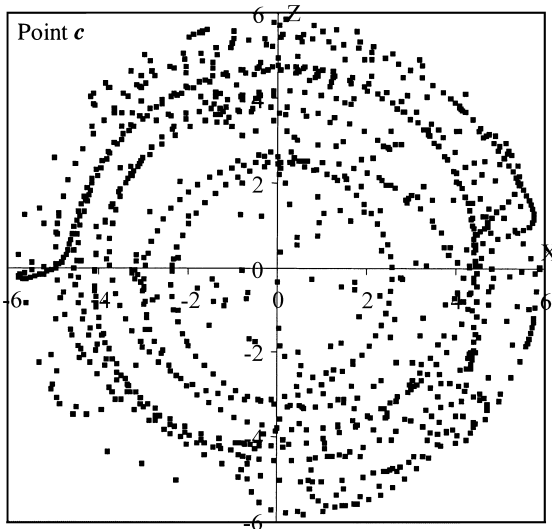


Fig. 11. The polishing trace pattern on the workpiece surface created by point c.

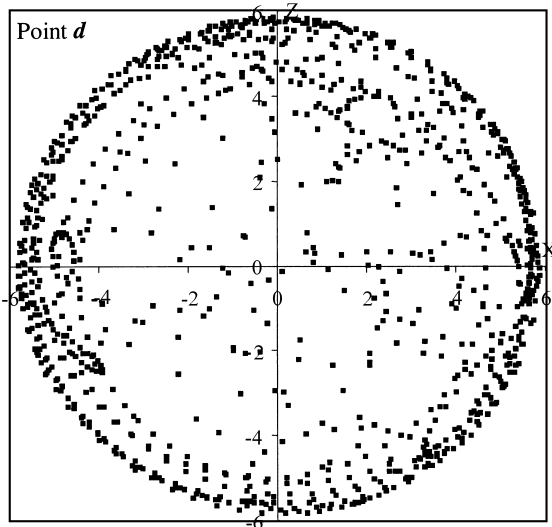


Fig. 12. The polishing trace pattern on the workpiece surface created by point d.

the traces superimposed, it would be possible to entirely cover the workpiece surface area. For a meaningful description of the polishing trace analysis, it is necessary to determine differences for different polishing parameters.

As shown in Figs. 9–12, the centre point on the polishing tool surface that makes a major contribution to the polishing

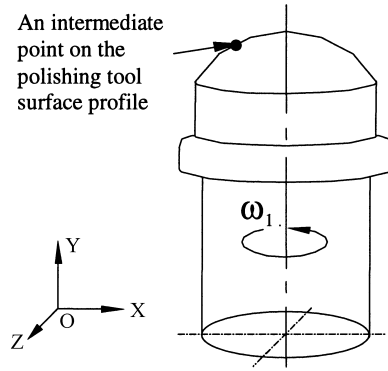


Fig. 14. Illustration of an intermediate point on the polishing tool surface.

of the workpiece centre area, and the edge point makes a greater contribution to polishing the workpiece edge area. Therefore, the frequencies of a specific point on the polishing tool passing the workpiece centre and edge surface areas are of major interest. This information may provide the rationale for selecting particular machine speeds that can address the missing zone problem at the centre or at the edge of the workpiece. For this to be achieved, it is necessary to divide the workpiece surface into multi-levels in the vertical Y-direction to allow a meaningful description of the polishing trace analysis. This is particularly useful when examining the relationship between the machine speed and the missing zones problem. Fig. 13 shows the multi-levels of the workpiece surface, where level 0 is at the centre of the workpiece surface on the top and the number of the level increases as the height, or the Y value, decreases.

Five different machine speeds ( $\omega_1=1200, 1350, 1500, 1650$  and  $1800$  rpm) were used to investigate the trace distribution created by a typical intermediate point of the polishing tool surface, as shown in Fig. 14. Figs. 15–19 show the projected view of the polishing trace patterns on the X–Z plane and the distribution trend at each level of the workpiece surface for each speed used. As is clear from the figures, a typical intermediate point of the polishing tool surface contributes less than to other areas polishing either the centre or the edge areas of the workpiece surface. However, the trace point at each level shows the differences due to the different machine speeds being used.

Further analysis of the trace point distribution, at different speeds, on the workpiece surface centre and edge areas may yield an estimate of the optimal polishing machine speed

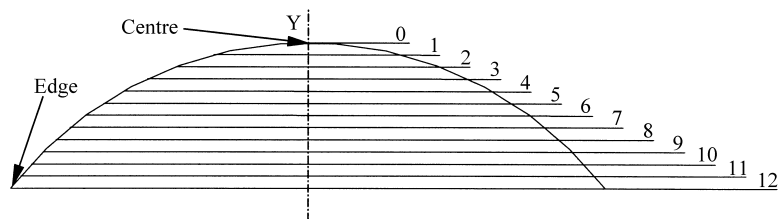


Fig. 13. Illustration of Y-level scaling of workpiece surface.

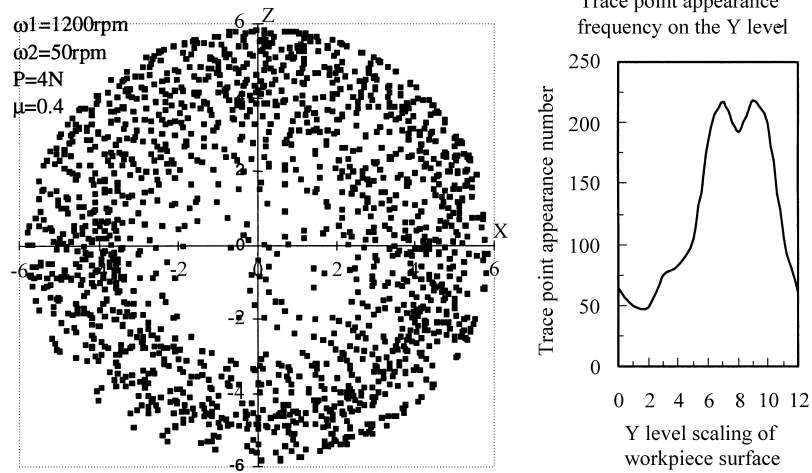


Fig. 15. The polishing trace on the workpiece surface ( $\omega_1=1200$  rpm).

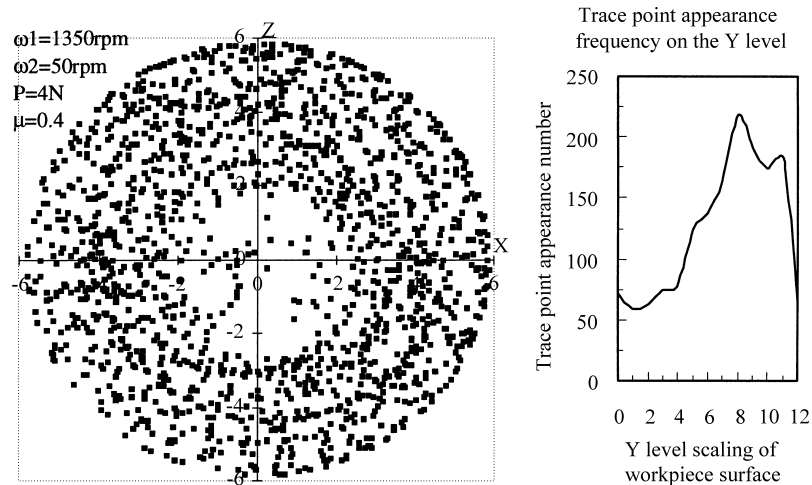


Fig. 16. The polishing trace on the workpiece surface ( $\omega_1=1350$  rpm).

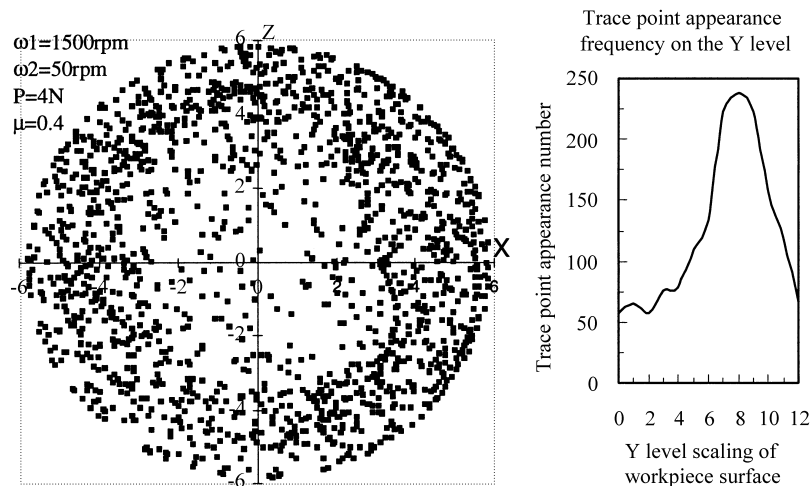


Fig. 17. The polishing trace on the workpiece surface ( $\omega_1=1500$  rpm).

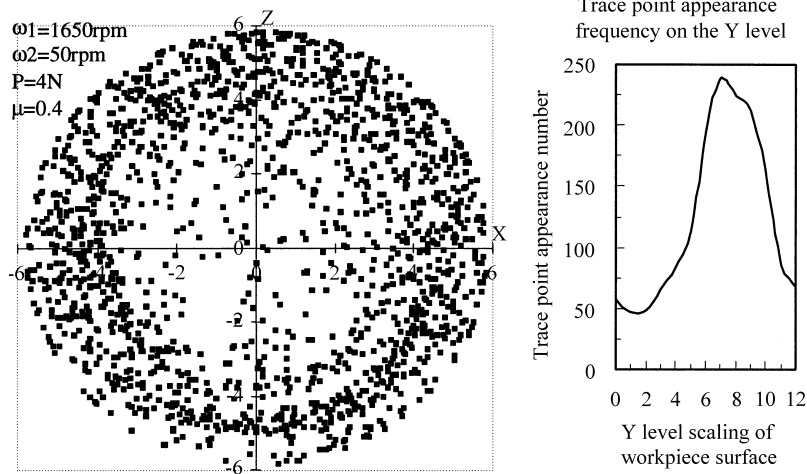


Fig. 18. The polishing trace on the workpiece surface ( $\omega_1=1650$  rpm).

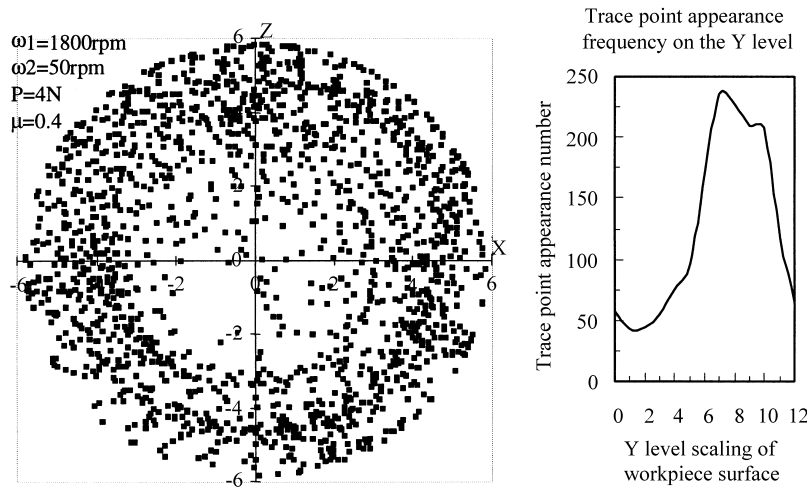


Fig. 19. The polishing trace on the workpiece surface ( $\omega_1=1800$  rpm).

needed for these conditions. Among the 1600 trace points for each speed, 43 is the lowest trace point frequency incidence that occurred at level 1 with 1800 rpm as the machine speed. If this lowest frequency incidence is set as a base unit, the plot of trace frequency against the machine speed used clearly indicates the varying trends of polishing trace point distribution with machine speed. Figs. 20 and 21 show the trends at the centre and edge areas of the workpiece surface, respectively. As shown in Fig. 20, the machine speed of 1350 rpm appears to be a turning point where, as the machine speed increases, the polishing trace point frequency incidence decreases rapidly at levels 0, 1 and 3. Level 2 shows a slightly different behaviour between 1500 and 1650 rpm. The variations in trace frequencies with respect to machine speed are significant and suggest that 1350 rpm is an appropriate speed to minimise the problem of the missing central zone. This speed produces a higher likelihood of polishing the centre area, compared with other speeds used.

Fig. 21 shows the polishing trace point distribution at the edge area of the workpiece surface. At level 11, the same trend can be seen as described above except for speeds 1650

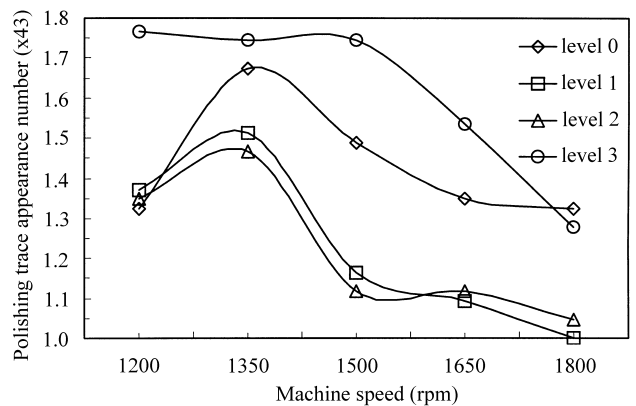


Fig. 20. Trace distribution analysis on centre area of workpiece surface.

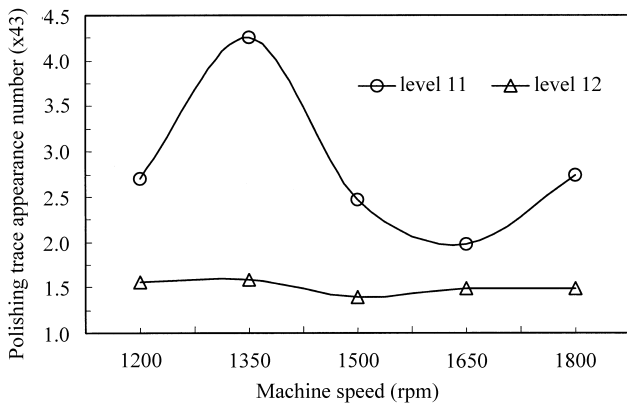


Fig. 21. Trace distribution analysis on edge area of workpiece surface.

and 1800 rpm. At level 12, it is hard to discern any significant difference, but the 1350 rpm speed still produces a slightly higher trace frequency value than other speeds. Hence 1350 rpm is still considered an appropriate speed to minimise the problem of the missing edge zone.

According to the results of the polishing trace analysis, the appropriate speed setting should be between 1200 and 1350 rpm. This is not so consistent with the experimental conclusion, which indicated that 1500 rpm was the best setting to produce a good surface [6]. However, considering various assumptions made in the present theoretical modelling, the agreement between the two results is reasonably close.

#### 4. Conclusions

A computational study was carried out for the precision optical lens polishing process. The problems associated with the polishing tool and workpiece contact behaviour during the polishing processes have been analysed. The computational results provide an insight into the contact status of the polishing process. Through the modelling process adopted in this work, the polishing load distribution and spatial polishing trace on the workpiece surface during the polishing process have been obtained.

The analysis of the polishing load distribution on the contact surface provided information about the relationship between contact area ratio and contact pressure. The results indicated that if contact pressure was distributed evenly on

the contact surface during the process, then the entire surface area could be evenly swept. Conversely, if the contact pressure distribution was uneven on the contact surface at the completion of all polishing cycles, it may be difficult to achieve geometrical accuracy and polishing quality for the workpiece over the polishing process.

Four points on the polishing tool surface were analysed and typical polishing trace patterns were produced on the workpiece surface. The centre point on the polishing tool surface made the major contribution to polishing the workpiece centre area, and the point at the edge made a greater contribution to polishing the workpiece edge area. Extended analyses of traces, using a multi-level subdivision of the workpiece surface, were performed to investigate the trace point distribution at each level. A typical intermediate point on the polishing tool surface was used. Comparison was made for traces using different machine speeds. It was shown that the appropriate speed setting should be between 1200 and 1350 rpm. This result is lower than the experimentally determined speed of 1500 rpm, but it is considered to be within an acceptable range.

#### Acknowledgements

The authors would like to thank the Australian Research Council and Eycon Lens Laboratories Pty. Ltd. for their financial support for this research project. The authors also thank Dr. Lin Ye and Dr. Lynne E. Bilston, Department of Mechanical and Mechatronic Engineering, Sydney University, for providing free access to their workstations.

#### References

- [1] K.L. Johnson, *Contact Mechanics*, Cambridge University Press, New York, 1985, p. 542.
- [2] D.A. Hill, D. Nowell, A. Sackfield, *Mechanics of Elastic Contact*, Butterworth-Heinemann, London, 1993, pp. 39–42.
- [3] O.C. Zienkiewicz, R.L. Taylor, *The Finite Element Method*, Vol. 2, 4th Edition, McGraw-Hill, London, 1991, pp. 159–184.
- [4] ABAQUS Theory Manual, Version 5.4, Hibbitt, Karlsson & Sorensen Inc., USA, 1994, pp. 3.2.1–3.2.3.
- [5] T.J.R. Hughes, J. Winget, Finite rotation effects in numerical integration of rate constitutive equations arising in large deformation analysis, *Int. J. Numer. Meth. Eng.* 15 (1980) 1862–1867.
- [6] J. Sun, *Polishing process for contact lenses*, Ph.D. Thesis, The University of Sydney, Sydney, NSW, 1998, pp. 53–93.